

## CONDENSED MATTER PHYSICS

## Superconducting pairing of topological surface states in bismuth selenide films on niobium

David Flötotto,<sup>1</sup> Yuichi Ota,<sup>2</sup> Yang Bai,<sup>1</sup> Can Zhang,<sup>1</sup> Koza Okazaki,<sup>2</sup> Akihiro Tsuzuki,<sup>2</sup> Takahiro Hashimoto,<sup>2</sup> James N. Eckstein,<sup>1</sup> Shik Shin,<sup>2</sup> Tai-Chang Chiang<sup>1\*</sup>

A topological insulator film coupled to a simple isotropic s-wave superconductor substrate can foster helical pairing of the Dirac fermions associated with the topological surface states. Experimental realization of such a system is exceedingly difficult, however using a novel “flip-chip” technique, we have prepared single-crystalline Bi<sub>2</sub>Se<sub>3</sub> films with predetermined thicknesses in terms of quintuple layers (QLs) on top of Nb substrates fresh from in situ cleavage. Our angle-resolved photoemission spectroscopy (ARPES) measurements of the film surface disclose superconducting gaps and coherence peaks of similar magnitude for both the topological surface states and bulk states. The ARPES spectral map as a function of temperature and film thickness up to 10 QLs reveals key characteristics relevant to the mechanism of coupling between the topological surface states and the superconducting Nb substrate; the effective coupling length is found to be much larger than the decay length of the topological surface states.

## INTRODUCTION

Topological superconductivity with p-wave-like pairing and time-reversal symmetry is one of the most intriguing topics of today's physics research due to its potential to host exotic phenomena such as Majorana fermions and supersymmetry, as well as potential applications in topological quantum computation (1–4). However, bulk topological superconductors (SCs) are rare and typically exhibit extremely small superconducting gaps and very low transition temperatures (4), which impede experimental observations of the predicted fascinating physics. A promising alternative route to realize topological superconductors is to fabricate artificial heterostructures of an SC and a topological insulator (TI), in which proximity coupling induces a  $p \pm ip$  pairing into the spin- and momentum-locked topological boundary states (1). Proximity-induced superconductivity in Bi<sub>2</sub>Se<sub>3</sub> and Bi<sub>2</sub>Te<sub>3</sub> has been reported by scanning tunneling microscopy and transport measurements (5–8). However, because of the simultaneous presence of surface and bulk states (BSs) at the Fermi level of these TIs, the occurrence of a helical Cooper pairing in the topological surface states (TSSs) has not been uniquely established. Unambiguous evidence can come, instead, from momentum-resolved probing techniques such as angle-resolved photoemission spectroscopy (ARPES). So far, proximity-induced pairing has been demonstrated only for the Bi<sub>2</sub>Se<sub>3</sub>/NbSe<sub>2</sub> heterostructure (9), but not for Bi<sub>2</sub>Se<sub>3</sub>/Bi<sub>2</sub>Sr<sub>2</sub>CaCu<sub>2</sub>O<sub>8+δ</sub>, though it was initially proposed by Wang *et al.* (10). The latter case involves growing Bi<sub>2</sub>Se<sub>3</sub> films on an orthorhombic d-wave SC (11, 12). The reason for these differences is still not well understood, but various factors have been cited, including strong electron correlation, Fermi surface and lattice structural mismatch, short superconducting coherence length, and a high density of structural defects at the interface (11–15). To resolve the issues, and thus to engineer optimized TI/SC heterostructures, it is critical to explore additional, preferably simple systems. However, practical difficulties with epitaxial growth of ultrathin Bi<sub>2</sub>Se<sub>3</sub> films on superconducting substrates and pronounced interface reactivity have, so far, limited the preparation of TI/SC heterostructures suitable for ARPES studies.

Here, we present ARPES results on the superconducting proximity effect as a function of temperature and TI film thickness for the

system Bi<sub>2</sub>Se<sub>3</sub>/Nb, which is arguably the simplest case in terms of the electronic and chemical structures of the components. Bi<sub>2</sub>Se<sub>3</sub> is a prototypical TI, whereas Nb is an isotropic s-wave SC with a coherence length of 380 Å and the highest transition temperature of  $T_C = 9.4$  K among all atomic elements. Because Nb is highly reactive and has a large lattice mismatch with Bi<sub>2</sub>Se<sub>3</sub>, standard Bi<sub>2</sub>Se<sub>3</sub> film growth conditions involving a high substrate temperature and a high Se overpressure cannot yield a single-crystalline Bi<sub>2</sub>Se<sub>3</sub> film on Nb with a sharp interface. Rather, the resulting system would be a Nb/NbSe<sub>2</sub>/Bi<sub>2</sub>Se<sub>3</sub> sandwich system with a complex mixed interfacial structure that would impede a detailed momentum-resolved characterization of the electronic structure. To circumvent this problem, we have developed a novel, generally applicable flip-chip preparation technique that, upon cleavage, yields a clean, ultrathin Bi<sub>2</sub>Se<sub>3</sub> film of a predetermined thickness and crystallographic orientation on a Nb substrate.

## RESULTS

Preparation and characterization of Bi<sub>2</sub>Se<sub>3</sub>/Nb heterostructures

In our experiment, Bi<sub>2</sub>Se<sub>3</sub>(0001) films with thicknesses of 4 to 10 quintuple layers (QLs) are epitaxially grown onto clean Al<sub>2</sub>O<sub>3</sub>(0001) substrates. Subsequently, 600 Å-thick polycrystalline Nb films are sputter-deposited on top of each of the Bi<sub>2</sub>Se<sub>3</sub> films at ~30°C. The resulting specimens are then broken into small pieces, flipped over, and glued with the Nb surfaces downward onto polished copper sheets using Ag epoxy. Finally, the Al<sub>2</sub>O<sub>3</sub> substrate backsides (now on top of the samples) are topped with cleavage pins (Fig. 1A). Each assembled sample is introduced into the ARPES system and cleaved in situ by pushing the pin sideways (Fig. 1B). As evidenced by our detailed analysis shown in Fig. 1 (C to E) (see the Supplementary Materials for details), the cleavage occurs at the Bi<sub>2</sub>Se<sub>3</sub>/Al<sub>2</sub>O<sub>3</sub> interface as the weakest link in the structure, thus exposing Bi<sub>2</sub>Se<sub>3</sub> films of thicknesses predetermined by the growth process.

## Momentum-resolved measurement of the superconducting gap

ARPES maps near the zone center are recorded in the temperature range of 1.5 to 13 K for all samples. Examples of these are shown in Fig. 2 for the 10- and 4-QL films exhibiting TSSs and partially filled

Copyright © 2018  
The Authors, some  
rights reserved;  
exclusive licensee  
American Association  
for the Advancement  
of Science. No claim to  
original U.S. Government  
Works. Distributed  
under a Creative  
Commons Attribution  
NonCommercial  
License 4.0 (CC BY-NC).

Downloaded from <http://advances.sciencemag.org/> on March 15, 2019

<sup>1</sup>Department of Physics and Frederick Seitz Materials Research Laboratory, University of Illinois, Urbana, IL 61801, USA. <sup>2</sup>Institute for Solid State Physics, The University of Tokyo, Kashiwa, Chiba, Japan.

\*Corresponding author. Email: tcchiang@illinois.edu

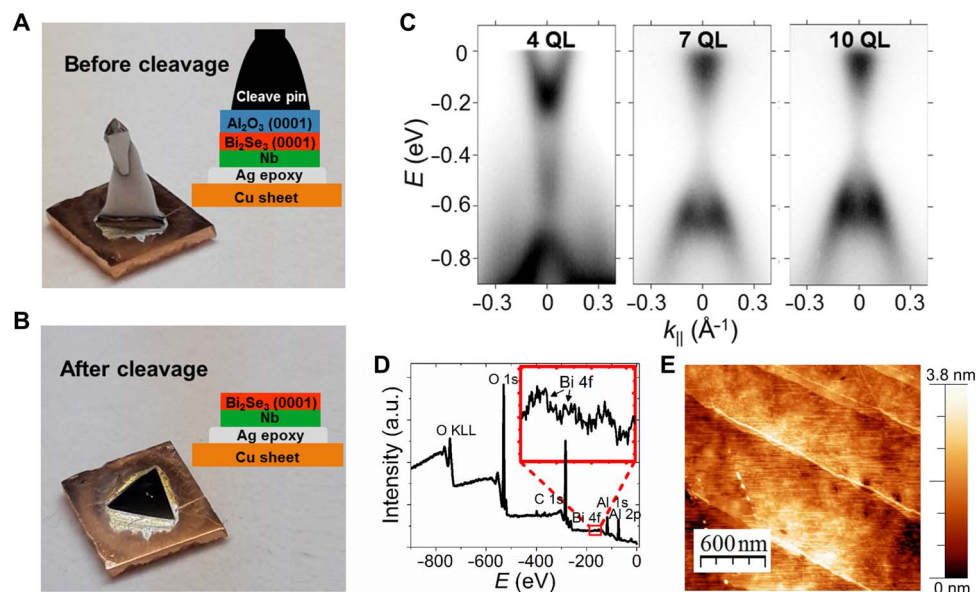


**Fig. 1. Cleavage-based sample preparation and characterization.** (A) Photo and schematic diagram of assembled  $\text{Bi}_2\text{Se}_3(0001)/\text{Nb}$  sample structure before cleavage. (B) Same sample structure after cleavage exposing a “fresh” surface of the  $\text{Bi}_2\text{Se}_3$  film with a predetermined thickness of four QLs. (C) ARPES maps for samples with 4, 7, and 10 QLs of  $\text{Bi}_2\text{Se}_3$  films. The spectra were recorded at photon energies of 18, 35, and 35 eV, respectively. (D) An x-ray photoelectron spectroscopy spectrum taken from a cleaved-off  $\text{Al}_2\text{O}_3$  substrate reveals that only a trace amount of Bi is left on the substrate after cleavage, thus confirming that the cleavage occurs at the  $\text{Bi}_2\text{Se}_3/\text{Al}_2\text{O}_3$  interface. (E) Atomic force microscopy (AFM) image of the  $\text{Bi}_2\text{Se}_3$  film surface after cleavage. The step structure corresponds well to that of the  $\text{Al}_2\text{O}_3$  substrate. a.u., arbitrary units.

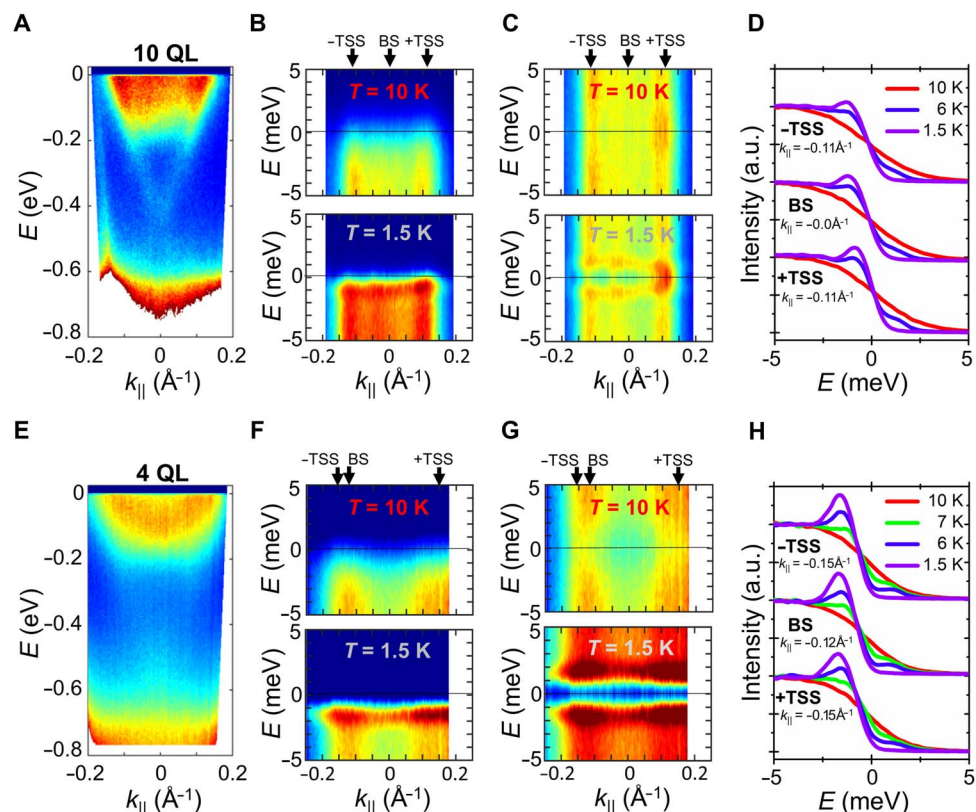


**Fig. 2. ARPES maps revealing proximity-induced superconductivity.** (A) ARPES map taken from a sample with a 10-QL  $\text{Bi}_2\text{Se}_3$  film at  $T = 10$  K using 6.994-eV photons. It shows a Dirac cone from the TSSs within the bulk band gap. (B) Detailed ARPES maps for energies close to the Fermi level for the 10-QL film sample at  $T = 10$  and 1.5 K, respectively. (C) Corresponding symmetrized ARPES maps reveal coherence peaks and superconducting gaps throughout momentum space at 1.5 K. (D) EDCs at three selected momenta corresponding to a BS, +TSS, and -TSS demonstrate proximity-induced superconductivity in all of these states. (E-H) Similar results for a sample with a four-QL  $\text{Bi}_2\text{Se}_3$  film.

bulk conduction bands at the Fermi level (Fig. 2, A and E). At  $T = 10$  K, the maps reveal thermally broadened Fermi edges, whereas at  $T = 1.5$  K, leading edge shifts and coherence peaks are observed (Fig. 2, B and F). The development of the superconducting gap is evident in the spectra obtained by symmetrization with respect to the Fermi level (Fig. 2, C and G). In particular, the energy distribution curves (EDCs) at three selected in-plane momentum positions corresponding to a BS and the spin- and momentum-locked TSSs ( $\pm$ TSSs) at the Fermi level clearly show coherence peaks of similar magnitude (Fig. 2, D and H). Thus, our measurements demonstrate that the proximity effect induces superconductivity into the BSs and the helical Dirac electrons of the TSSs, as proposed by Fu and Kane (1).

### Proximity-induced superconductivity as a function of TI film thickness and temperature

Figure 3 shows the symmetrized EDCs associated with BS, +TSS, and -TSS of the  $\text{Bi}_2\text{Se}_3$  films of different thicknesses, and that of a bare Nb reference sample. For all samples, the height of the coherence peaks and the size of the superconducting gap increase with decreasing temperature below  $T_C^{\text{Nb}}$ , and both superconducting features become less pronounced with increasing TI film thicknesses at a given temperature below  $T_C^{\text{Nb}}$ . To further quantify the proximity effect, we fit the symmetrized EDCs by a Dynes function (black curves), which yields the superconducting gap  $\Delta(T)$  as a function of temperature for each case (Fig. 4A). The results for BS and the averaged results for  $\pm$ TSS (denoted  $\langle$ TSS $\rangle$  below) are well described by the BCS mean-field equation (dashed curves in Fig. 4A)

$$\Delta(T) = \Delta(0) \tanh \left( A \sqrt{\frac{T_C}{T} - 1} \right) \quad (1)$$

where  $A = 1.74$ . Our analysis reveals that the superconducting transition temperatures for BS and  $\langle$ TSS $\rangle$  are independent of film thickness and, within the experimental error, equal to  $T_C^{\text{Nb}}$ . Physically, Cooper pairs are induced into the bulk bands of the  $\text{Bi}_2\text{Se}_3$  films through Andreev reflection at the interface. Thus, the pair density is finite for  $T < T_C$  but drops to zero when Andreev reflection ceases for  $T > T_C$ . Another important observation is that the zero-temperature gap,  $\Delta(0)$ , decreases as a function of film thickness (Fig. 4B), and the decay behavior is the same for BS and  $\langle$ TSS $\rangle$ . The decay can be understood in general terms as follows. Quasi-particles induced in the TI film by Andreev reflection lose their phase coherence away from the interface (16), and thus, the Cooper pair density and, accordingly, the proximity-induced gap probed near the  $\text{Bi}_2\text{Se}_3$  film surface decrease with increasing TI film thickness in accordance with theoretical predictions (see the Supplementary Materials) (14, 17, 18). A fit of the observed decay of  $\Delta(0)$  by an exponential function

$$\Delta(0) = \Delta_{\text{Nb}} \exp(-d/\lambda) \quad (2)$$

where  $\Delta_{\text{Nb}}$  is the zero-temperature gap of bare Nb,  $d$  is the  $\text{Bi}_2\text{Se}_3$  film thickness, and  $\lambda$  is the decay length, yields the dashed curve in Fig. 4B. The decay length  $\lambda = 8.4$  QLs deduced from the fit is a measure of the quasi-particle coherence length associated with Andreev reflections. The results can also be analyzed in terms of more elaborate models that

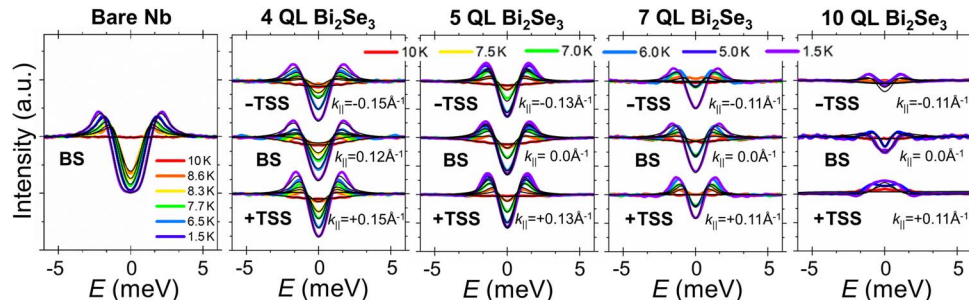


**Fig. 3. Symmetrized ARPES EDCs as a function of temperature and  $\text{Bi}_2\text{Se}_3$  film thickness.** Results for a bare Nb sample as well as for BS, +TSS, and -TSS at  $\text{Bi}_2\text{Se}_3$  film thicknesses of 4, 5, 7, and 10 QL, respectively. The height of the coherence peaks and the size of the superconducting gap increase with decreasing temperature below  $T_C^{\text{Nb}}$  and completely vanish for temperatures above  $T_C^{\text{Nb}}$ ; both superconducting features become less pronounced for increasing  $\text{Bi}_2\text{Se}_3$  film thicknesses at a given temperature below  $T_C^{\text{Nb}}$ .

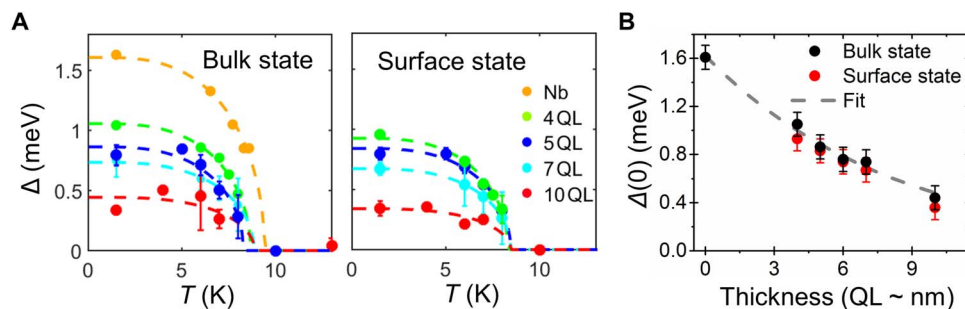


**Fig. 4. Extracted superconducting gaps for the BSs and TSSs.** (A) Superconducting gaps for the BS and the TSS as a function of temperature deduced from fitting the symmetrized EDCs with a Dynes function. Results for different film thicknesses and a bare Nb sample are shown. The curves are fit using Eq. 1; the fits yield the zero-temperature gap  $\Delta(0)$  for each case. (B)  $\Delta(0)$  for a BS and  $\langle$ TSS $\rangle$  as a function of film thickness. The curve is an exponential fit.

consider various scattering and dephasing mechanisms in greater detail. An analysis based on a commonly used quasi-classical Usadel model (17) is shown in the Supplementary Materials; the decay seen in Fig. 4B can be fitted equally well by a  $1/d^2$  dependence based on this model. Our available data do not allow a quantitative distinction between the two different fits.

## DISCUSSION

Notably, and in contrast to previous reports (9), our study shows that the above findings hold for both the BSs and the TSSs. The identical decay behavior of  $\Delta(0)$  with increasing film thickness for both the BSs and TSSs (Fig. 4B) has a strong implication regarding the details of the induced pairing. Because the wave functions associated with the TSSs are concentrated near the surface with an exponential decay length of less than two QLs (19), direct transfer of Cooper pairs from the interface to the TI film surface by tunneling decays rapidly with increasing thickness and is negligible for film thicknesses greater than or equal to seven QLs (20). However, even the TSSs of the 10-QL samples exhibit the same gap as the BSs. This suggests that the TSSs and BSs are quantum-mechanically coupled together, and thus, any superconducting properties impressed upon the BSs are transferred to the TSSs. This happens, although the Cooper pairing in the TSSs and the BSs have very different characters, because the TSSs are analytic continuations of the BSs in energy-momentum space and both are quantum-mechanically coherent over a length scale determined by the mean free paths of the associated quasi-particles (21). Evidently, the quasi-particle mean free paths in the  $\text{Bi}_2\text{Se}_3$  films are sufficiently large for the BSs and TSSs to exhibit the same gap over the entire range of film thickness studied.

The observed proximity-induced gaps in the BSs and the TSSs of  $\text{Bi}_2\text{Se}_3$  are significantly larger than those reported for  $\text{Bi}_2\text{Se}_3$  and  $\text{Bi}_2\text{Te}_3$  films of similar film thickness on  $\text{NbSe}_2$  substrates (5, 6, 9) because of the larger pairing potential induced by Nb (1.6 meV) than by  $\text{NbSe}_2$  (1.2 meV) (5). Therefore, our study not only gives momentum-resolved insight into the superconducting proximity effect for the arguably simplest TI/SC system but also shows that, on the basis of our novel flip-chip sample preparation technique, optimized artificial topological SCs with a sizable gap can be realized. This opens up new routes to explore the exotic physics in topological SCs and the superconducting proximity effects in general. For example, the flip-chip sample preparation technique will allow the controlled manipulation of the TI/SC interface with respect to defects and magnetic impurities at the interface created by light sputtering of the  $\text{Bi}_2\text{Se}_3$  surface and/or by deposition of impurities on the  $\text{Bi}_2\text{Se}_3$  surface before Nb film growth. This interfacial modification would not change the bulk crystal structure of the  $\text{Bi}_2\text{Se}_3$  film. By contrast, in the conventional approach of heteroepitaxial  $\text{Bi}_2\text{Se}_3$  film growth directly on an SC substrate, defects and impurities introduced on the SC substrate would surely have a negative impact on the TI film quality, because good epitaxial growth requires structural coherence. Thus, the flip-chip technique will permit the preparation of a wide range of other TI/SC systems suitable for ARPES studies, including SC compounds with larger gaps and higher  $T_C$ 's, as well as more complicated heterostructures of TI, SC, and ferromagnetic layers.

## MATERIALS AND METHODS

### $\text{Bi}_2\text{Se}_3/\text{Nb}$ sample preparation

The epitaxial  $\text{Bi}_2\text{Se}_3(0001)$  films were grown by a “two-step process” onto in situ ozone-cleaned  $\text{Al}_2\text{O}_3(0001)$  substrates. A two-QL film

was grown first at a substrate temperature of 220°C, and subsequent deposition of additional QLs up to the desired film thickness was performed at a substrate temperature of 280°C. Each film was postannealed at 280°C for 3 hours under a low flux of Se to improve the film quality. The crystal structure and thickness of the  $\text{Bi}_2\text{Se}_3$  films were verified, as needed, by in situ reflection high-energy electron diffraction and ex situ x-ray diffraction. After the growth of each  $\text{Bi}_2\text{Se}_3$  film, a 600 Å (110) textured polycrystalline Nb film was sputter-deposited on top at an Ar gas pressure of 6 mtorr and a power level of 150 W. The deposition was performed at room temperature to avoid interdiffusion at the interface (22). Each sample was glued upside down on a polished copper sheet using a low-temperature-curing Ag epoxy; a cleavage post was mounted on the backside of the  $\text{Al}_2\text{O}_3$  substrate with Torr Seal, which was cured at 60°C for 3 hours.

### ARPES measurements

Most of the ARPES measurements were performed using a laser-based ARPES system (base pressure,  $4 \times 10^{-11}$  mbar) at the Institute for Solid State Physics at The University of Tokyo. The system was equipped with a Scienta HR8000 hemispherical analyzer, a vacuum ultraviolet laser with a photon energy of 6.994 eV, and a sample manipulator cooled by (superfluid) liquid helium. The sample temperature was varied in the range of 1.5 to 13 K. This setup provides an experimental energy resolution of 1.2 meV and a stability of the Fermi edge of  $\sim 0.1$  meV, as verified by following the procedures established previously (23) [see the Supplementary Materials and the study of Ota *et al.* (24) for further details about the laser-ARPES apparatus and standard testing procedures]. Some additional ARPES measurements were performed using photon energies in the range of 18 to 52 eV at the One-Cube Beamline at BESSY II, as well as beamline 4.03 at the Advanced Light Source (ALS) at Berkeley (see the Supplementary Materials).

### SUPPLEMENTARY MATERIALS

Supplementary material for this article is available at <http://advances.sciencemag.org/cgi/content/full/4/4/ear7214/DC1>

- section S1. Characterization of as-grown  $\text{Bi}_2\text{Se}_3$  films
- section S2. Characterization of cleaved  $\text{Bi}_2\text{Se}_3/\text{Nb}$  samples
- section S3. Stability and accuracy for measuring the Fermi level  $E_F$  and the gap
- section S4. Comparison to a model calculation
- section S5. ARPES measurements of the superconducting proximity effect at the One-Cube Beamline at BESSY II
- fig. S1. Characterization of as-grown  $\text{Bi}_2\text{Se}_3$  films.
- fig. S2. ARPES maps of a seven-QL  $\text{Bi}_2\text{Se}_3/\text{Nb}$  sample.
- fig. S3. Surface morphology of cleaved  $\text{Bi}_2\text{Se}_3/\text{Nb}$  samples.
- fig. S4. Superconducting gap of Nb as a function of detector angular channels.
- fig. S5. Superconducting gaps as a function of film thickness.
- fig. S6. ARPES results obtained at the One-Cube Beamline at BESSY II.
- References (25–27)

### REFERENCES AND NOTES

1. L. Fu, C. L. Kane, Superconducting proximity effect and Majorana fermions at the surface of a topological insulator. *Phys. Rev. Lett.* **100**, 096407 (2008).
2. T. Grover, D. N. Sheng, A. Vishwanath, Emergent space-time supersymmetry at the boundary of a topological phase. *Science* **344**, 280–283 (2014).
3. Y. Ando, L. Fu, Topological crystalline insulators and topological superconductors: From concepts to materials. *Annu. Rev. Condens. Matter Phys.* **6**, 361–381 (2015).
4. M. Sato, Y. Ando, Topological superconductors: A review. *Rep. Prog. Phys.* **80**, 076501 (2017).
5. J.-P. Xu, C. Liu, M.-X. Wang, J. Ge, Z.-L. Liu, X. Yang, Y. Chen, Y. Liu, Z.-A. Xu, C.-L. Gao, D. Qian, F.-C. Zhang, J.-F. Jia, Artificial topological superconductor by the proximity effect. *Phys. Rev. Lett.* **112**, 217001 (2014).

6. M.-X. Wang, C. Liu, J.-P. Xu, F. Yang, L. Miao, M.-Y. Yao, C. L. Gao, C. Shen, X. Ma, X. Chen, Z.-A. Xu, Y. Liu, S.-C. Zhang, D. Qian, J.-F. Jia, Q.-K. Xue, The coexistence of superconductivity and topological order in the  $\text{Bi}_2\text{Se}_3$  thin films. *Science* **336**, 52–55 (2012).
7. P. Zareapour, A. Hayat, S. Y. F. Zhao, M. Kreshchuk, A. Jain, D. C. Kwok, N. Lee, S.-W. Cheong, Z. Xu, A. Yang, G. D. Gu, S. Jia, R. J. Cava, K. S. Burch, Proximity-induced high-temperature superconductivity in the topological insulators  $\text{Bi}_2\text{Se}_3$  and  $\text{Bi}_2\text{Te}_3$ . *Nat. Commun.* **3**, 1056 (2012).
8. M. Q. He, J. Y. Shen, A. P. Petrović, Q. L. He, H. C. Liu, Y. Zheng, C. H. Wong, Q. H. Chen, J. N. Wang, K. T. Law, I. K. Sou, R. Lortz, Pseudogap and proximity effect in the  $\text{Bi}_2\text{Te}_3/\text{Fe}_{1+y}\text{Te}$  interfacial superconductor. *Sci. Rep.* **6**, 32508 (2016).
9. S.-Y. Xu, N. Alidoust, I. Belopolski, A. Richardella, C. Liu, M. Neupane, G. Bian, S.-H. Huang, R. Sankar, C. Fang, B. Dellabetta, W. Dai, Q. Li, M. J. Gilbert, F. Chou, N. Samarth, M. Z. Hasan, Momentum-space imaging of Cooper pairing in a half-Dirac-gas topological superconductor. *Nat. Phys.* **10**, 943–950 (2014).
10. E. Wang, H. Ding, A. V. Fedorov, W. Yao, Z. Li, Y.-F. Lv, K. Zhao, L.-G. Zhang, Z. Xu, J. Schneeloch, R. Zhong, S.-H. Ji, L. Wang, K. He, X. Ma, G. Gu, H. Yao, Q.-K. Xue, X. Chen, S. Zhou, Fully gapped topological surface states in  $\text{Bi}_2\text{Se}_3$  films induced by a  $d$ -wave high-temperature superconductor. *Nat. Phys.* **9**, 621–625 (2013).
11. S.-Y. Xu, C. Liu, A. Richardella, I. Belopolski, N. Alidoust, M. Neupane, G. Bian, N. Samarth, M. Z. Hasan, Fermi-level electronic structure of a topological-insulator/cuprate-superconductor based heterostructure in the superconducting proximity effect regime. *Phys. Rev. B* **90**, 085128 (2014).
12. T. Yilmaz, I. Pletikosić, A. P. Weber, J. T. Sadowski, G. D. Gu, A. N. Caruso, B. Sinkovic, T. Valla, Absence of a proximity effect for a thin-film of a  $\text{Bi}_2\text{Se}_3$  topological insulator grown on top of a  $\text{Bi}_2\text{Sr}_2\text{CaCu}_2\text{O}_{8+\delta}$  cuprate superconductor. *Phys. Rev. Lett.* **113**, 067003 (2014).
13. W.-J. Li, S.-P. Chao, T.-K. Lee, Theoretical study of large proximity-induced  $s$ -wave-like pairing from a  $d$ -wave superconductor. *Phys. Rev. B* **93**, 035140 (2016).
14. C. R. Reeg, D. L. Maslov, Hard gap in a normal layer coupled to a superconductor. *Phys. Rev. B* **94**, 020501 (2016).
15. C.-K. Chiu, W. S. Cole, S. Das Sarma, Induced spectral gap and pairing correlations from superconducting proximity effect. *Phys. Rev. B* **94**, 125304 (2016).
16. T. M. Klapwijk, Proximity effect from an Andreev perspective. *J. Supercond.* **17**, 593–611 (2004).
17. W. Belzig, C. Bruder, G. Schön, Local density of states in a dirty normal metal connected to a superconductor. *Phys. Rev. B* **54**, 9443–9448 (1996).
18. S. Pilgram, W. Belzig, C. Bruder, Excitation spectrum of mesoscopic proximity structures. *Phys. Rev. B* **62**, 12462–12467 (2000).
19. X. Wang, T.-C. Chiang, Topological states in  $\text{Bi}_2\text{Se}_3$  surfaces created by cleavage within a quintuple layer: Analysis in terms of the Shockley criterion. *Phys. Rev. B* **89**, 125109 (2014).
20. Y. Zhang, K. He, C.-Z. Chang, C.-L. Song, L.-L. Wang, X. Chen, J.-F. Jia, Z. Fang, X. Dai, W.-Y. Shan, S.-Q. Shen, Q. Niu, X.-L. Qi, S.-C. Zhang, X.-C. Ma, Q.-K. Xue, Crossover of the three-dimensional topological insulator  $\text{Bi}_2\text{Se}_3$  to the two-dimensional limit. *Nat. Phys.* **6**, 584–588 (2010).
21. K. Saha, I. Garate, Theory of bulk-surface coupling in topological insulator films. *Phys. Rev. B* **90**, 245418 (2014).
22. N. de Jong, E. Frantzeskakis, B. Zwartsenberg, Y. K. Huang, D. Wu, P. Hlawenka, J. Sánchez-Barriga, A. Varykhalov, E. van Heumen, M. S. Golden, Angle-resolved and core-level photoemission study of interfacing the topological insulator  $\text{Bi}_{1.5}\text{Sb}_{0.5}\text{Te}_{1.7}\text{Se}_{1.3}$  with Ag, Nb, and Fe. *Phys. Rev. B* **92**, 075127 (2015).
23. Y. Ota, K. Okazaki, H. Q. Yamamoto, T. Yamamoto, S. Watanabe, C. Chen, M. Nagao, S. Watauchi, I. Tanaka, Y. Takano, S. Shin, Unconventional superconductivity in the  $\text{BiS}_2$ -based layered superconductor  $\text{NdO}_{0.71}\text{F}_{0.29}\text{BiS}_2$ . *Phys. Rev. Lett.* **118**, 167002 (2017).
24. Y. Ota, K. Okazaki, Y. Kotani, T. Shimojima, W. Malaeb, S. Watanabe, C.-T. Chen, K. Kihou, C. H. Lee, A. Iyo, H. Eisaki, T. Saito, H. Fukazawa, Y. Kohori, S. Shin, Evidence for excluding the possibility of  $d$ -wave superconducting-gap symmetry in Ba-doped  $\text{KFe}_2\text{As}_2$ . *Phys. Rev. B* **89**, 081103 (2014).
25. Y. F. Lee, R. Kumar, F. Hunte, J. Narayan, J. Schwartz, Control of intrinsic defects and magnetotransport properties of  $\text{Bi}_2\text{Se}_3/c$ -sapphire epitaxial heterostructures. *Acta Mater.* **95**, 57–64 (2015).
26. R. C. Hatch, M. Bianchi, D. Guan, S. Bao, J. Mi, B. B. Iversen, L. Nilsson, L. Hornekaer, P. Hofmann, Stability of the  $\text{Bi}_2\text{Se}_3$ (111) topological state: Electron-phonon and electron-defect scattering. *Phys. Rev. B* **83**, 241303 (2011).
27. J. Dufouleur, L. Veyrat, B. Dassonneville, C. Nowka, S. Hampel, P. Leksin, B. Eichler, O. G. Schmidt, B. Büchner, R. Giraud, Enhanced mobility of spin-helical dirac fermions in disordered 3D topological insulators. *Nano Lett.* **16**, 6733–6737 (2016).

**Acknowledgments:** We are grateful to the beamline scientists D. Yevtushynsky and E. Rienks (One-Cube BL UE112-lowPGM-b+1<sup>3</sup>, BESSY II), as well as J. D. Denlinger (beamline 4.03, ALS) for providing support during the synchrotron-based ARPES measurements. **Funding:** We acknowledge that this work was partly carried out in the Central Research Facilities of the Frederick Seitz Materials Research Laboratory and supported by (i) the U.S. Department of Energy, Office of Science, Office of Basic Energy Sciences, Division of Materials Science and Engineering (grant no. DE-FG02-07ER46383 for T.-C.C. and award no. DE-AC02-07CH11358 for J.N.E.), (ii) the NSF (grant no. DMR 11-05998 for J.N.E.), (iii) the Deutsche Forschungsgemeinschaft (FL 974/1-1), and (iv) the Photon and Quantum Basic Research Coordinated Development Program from the Ministry of Education, Culture, Sports, Science and Technology, Japan, Japan Society for the Promotion of Science KAKENHI (grant no. JP25220707). **Author contributions:** D.F. and T.-C.C. organized the project. Y.O., K.O., A.T., T.H., and S.S. performed the laser ARPES measurements. Y.B., C.Z., and J.N.E. designed and prepared the samples. D.F. and Y.B. performed sample characterization and diagnosis by x-ray, AFM, and other measurements. D.F. carried out additional ARPES studies at BESSY II and ALS. **Competing interests:** The authors declare no competing interests. **Data and materials availability:** All data needed to evaluate the conclusions in the paper are present in the paper and/or the Supplementary Materials. Additional data related to this paper may be requested from T.-C.C. (tcchiang@illinois.edu).

Submitted 11 December 2017

Accepted 9 March 2018

Published 27 April 2018

10.1126/sciadv.aar7214

**Citation:** D. Flötotto, Y. Ota, Y. Bai, C. Zhang, K. Okazaki, A. Tsuzuki, T. Hashimoto, J. N. Eckstein, S. Shin, T.-C. Chiang, Superconducting pairing of topological surface states in bismuth selenide films on niobium. *Sci. Adv.* **4**, eaar7214 (2018).

## Superconducting pairing of topological surface states in bismuth selenide films on niobium

David Flötotto, Yuichi Ota, Yang Bai, Can Zhang, Kozo Okazaki, Akihiro Tsuzuki, Takahiro Hashimoto, James N. Eckstein, Shik Shin and Tai-Chang Chiang

*Sci Adv* 4 (4), eaar7214.  
DOI: 10.1126/sciadv.aar7214

ARTICLE TOOLS	<a href="http://advances.sciencemag.org/content/4/4/eaar7214">http://advances.sciencemag.org/content/4/4/eaar7214</a>
SUPPLEMENTARY MATERIALS	<a href="http://advances.sciencemag.org/content/suppl/2018/04/23/4.4.eaar7214.DC1">http://advances.sciencemag.org/content/suppl/2018/04/23/4.4.eaar7214.DC1</a>
REFERENCES	This article cites 27 articles, 2 of which you can access for free <a href="http://advances.sciencemag.org/content/4/4/eaar7214#BIBL">http://advances.sciencemag.org/content/4/4/eaar7214#BIBL</a>
PERMISSIONS	<a href="http://www.sciencemag.org/help/reprints-and-permissions">http://www.sciencemag.org/help/reprints-and-permissions</a>

Use of this article is subject to the [Terms of Service](#)

---

*Science Advances* (ISSN 2375-2548) is published by the American Association for the Advancement of Science, 1200 New York Avenue NW, Washington, DC 20005. 2017 © The Authors, some rights reserved; exclusive licensee American Association for the Advancement of Science. No claim to original U.S. Government Works. The title *Science Advances* is a registered trademark of AAAS.